Journal Pre-proofs

Engineering low-temperature ozone activation of zeolites: process specifics, possible mechanisms and hybrid activation methods

Julien Devos, Robin Borms, Sven Robijns, Gleb Ivanushkin, Ibrahim Khalil, Michiel Dusselier

PII: S1385-8947(21)05435-8
DOI: https://doi.org/10.1016/j.cej.2021.133862
Reference: CEJ 133862

To appear in: *Chemical Engineering Journal*

Received Date: 9 July 2021
Revised Date: 22 November 2021
Accepted Date: 23 November 2021

Please cite this article as: J. Devos, R. Borms, S. Robijns, G. Ivanushkin, I. Khalil, M. Dusselier, Engineering low-temperature ozone activation of zeolites: process specifics, possible mechanisms and hybrid activation methods, *Chemical Engineering Journal* (2021), doi: https://doi.org/10.1016/j.cej.2021.133862

This is a PDF file of an article that has undergone enhancements after acceptance, such as the addition of a cover page and metadata, and formatting for readability, but it is not yet the definitive version of record. This version will undergo additional copyediting, typesetting and review before it is published in its final form, but we are providing this version to give early visibility of the article. Please note that, during the production process, errors may be discovered which could affect the content, and all legal disclaimers that apply to the journal pertain.

© 2021 Elsevier B.V. All rights reserved.

Highlights:

- Ozonation in a low temperature flow removes zeolite organics
- Open zeolites were obtained without structural degradation.
- Boundary conditions heavily depend on the zeolitic properties.
- Mechanistic insights suggest internal diffusion bottlenecks
- An efficient hybrid/sequential OSDA removal method was demonstrated.

Engineering low-temperature ozone activation of zeolites: process specifics, possible mechanisms and hybrid activation methods

Julien Devos,† Robin Borms† Sven Robijns,† Gleb Ivanushkin,† Ibrahim Khalil,† and Michiel Dusselier*†

† Center for Sustainable Catalysis and Engineering (CSCE), KU Leuven, Celestijnenlaan 200F, B-3001 Leuven, Belgium.

Corresponding Author

* M.D.: michiel.dusselier@kuleuven.be

Keywords:

zeolites, ozone, detemplation, ozonation, calcination, low-temperature activation, ozonolysis, shrinking core model, zeolite engineering

Journal Pre-proofs

Graphical abstract

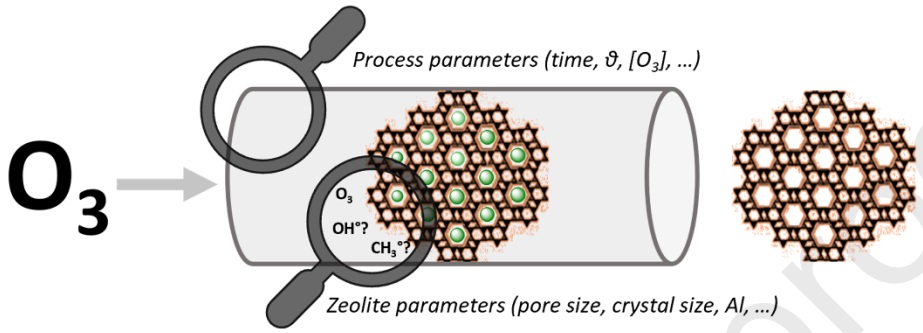

Journal Pre-proofs

ABSTRACT:

Zeolite activation is the first, but often overlooked, post-synthetic treatment needed to transform an as-made material into an adsorbent or catalyst. Ozonation at low temperatures provides an alternative for conventional calcination treatments, with important consequences for zeolite stability and acidity. While sometimes used in the context of emptying novel less thermally stable structures, a thorough look at ozonation for bulk zeolites is missing. Decomposition of organic structure-directing agents was achieved for three OSDA-zeolite systems yielding empty SSZ-13, ZSM-5 and β zeolites at select ozonation conditions. The effect of various process parameters, as well as synthetic parameters, were investigated. Infrared and mass spectrometry after alternating O_2-O_3 activation mode experiments provide some mechanistic insights into ozonation. The rate-limiting steps of both low-temperature ozonation and air calcinations can be circumvented by low-temperature ozonation after medium-temperature calcination.

Journal Pre-proofs

1. Introduction

Synthetic zeolites are used in a very wide range of applications, functioning as ion-exchangers or catalysts, as well as in separation technologies, thanks to their high versatility.[1,2] Some potentially very interesting structures of synthesized zeolites can, however, not be exploited due to their degradation upon thermal activation (e.g., zincosilicate RUB-17, Zn-RSN[3,4]). Furthermore, a part of the zeolitic acid sites can be transformed and lost upon (too strong) thermal activation.[5–8] Instead of conventional high-temperature activation (i.e., calcination), low temperature (<250°C, hereafter LT) activation could open up the possibility to avoid thermal damage while emptying, inspired by other LT-activation methods of mesoporous materials.[9,10] However, zeolitic pores are too tight for complete extractive removal of organic structure-directing agents (OSDA) without (partial) structural degradation. Chemical methods for LT activation (OSDA removal, also referred to herein as detemplation) can also be achieved via the radical degradation of encaged OSDA using strong oxidants, such as H_2O_2 (E° = 1.8 eV), O_3 (E° = 2.1 eV), and OH° (E° = 2.7 eV) that are generated via a variety of techniques (Fenton reagents,[8,11] UV-radiation,[8,12–14] corona discharge,[15–19] cold plasma,[20–23] or electron beam radiation[24]). Amongst these, gas-phase ozone-fed systems are promising systems for complete template removal (ozonation).[15–19] Most often, ozone is used as a tool to empty thermally less stable structures (e.g., activation of CIT-9[25]) or when the non-zeolite surroundings (e.g., polymeric membranes) do not allow high temperatures.[18] However, only a very limited set of conditions and a large dependence on the zeolitic properties have been reported. Additional mechanistic insights could foster process optimization and turn ozonation into a more generic and wider used technique. In ozone treatments, water (vapor) present in the gas feed is known to play a key role in OSDA oxidation, as hypothesized by Kuhn et al.[15] and later experimentally proven by Zhang et al.[18] In the presence of water, O_3 is said to decompose into smaller OH° intermediates which allows better diffusion into

(small pore) zeolites, leading to a higher oxidation potential. Important here is that hydroxyl radicals have only very short lifetimes.[26] Hence, they are ideally formed in-situ on the zeolite surface or within the pores for initiation and propagation of the complex chain reactions of oxidative OSDA degradation. In this aspect, it is interesting to note that O_3 decomposes easily on zeolites, especially on silanols.[27] The latter is likely due to ozone being a weaker Lewis base than water.[28] Take all together, the exact role of ozone during activation is unknown and a detailed mechanistic understanding is lacking, in part due to the non-specific and random behaviour of complex radical chain oxidations and its interaction with (sometimes mobile) zeolite constituents.[24] Yet, it is believed that an increased understanding of LT-OSDA removal mechanisms will foster optimization of ozonation (and vice-versa), enabling a new lever of post-synthetic control.

In this study, the process of OSDA removal using gas-phase ozone at a low temperature is investigated by means of single-parameter variations. Under a select set of conditions, the latter allows complete removal of all organic matter at low temperatures (<250°C), yielding intact empty zeolites. Compared to classical calcination, different rate-limiting steps are detected, requiring a careful match between ozonation set-up parameters with the textural, structural, and acid site properties of the zeolite. The fundamental insights on LT activation can be further exploited to more challenging OSDA-zeolite complexes and to develop scale-up at industrially relevant conditions.

2. Materials and methods:

2.1. Synthesis of zeolite precursors

Three OSDA-framework composites were synthesized via conventional hydrothermal crystallization methods: small pore SSZ-13 (**CHA**) containing trimethyladamantylammonium (TMAda), medium pore ZSM-5 (**MFI**) with tetrapropylammonium (TPA), and large pore

Journal Pre-proofs

zeolite beta (***BEA**) containing tetraethylammonium (TEA). Three different synthesis procedures were exploited (see section S1), each in a variety of batch compositions (see table S1). The 'amorphous source' and 'IZC' routes are hydroxide-based routes involving recipes, according to Devos *et al.*[29,30] The F-containing (BEA) syntheses are based on Camblor *et al.* [31] Most syntheses were made stoichiometrically identical with the following batch composition: $1SiO_2$:(0.025-0.067)Al:0.35($OSDA^+$+Na^+):0.35OH^- :12.5H_2O. Synthesized materials are labeled '*FTC[Si/Al$_B$;Na]**'. FTC (framework topology code) reflects the 3-letter code of the International Zeolite Association (IZA),[32] between brackets 'Si/Al$_B$' reflects the Si to Al ratio in the batch, and 'Na' is added in case sodium was added to the synthesis mixture. As a suffix, an asterisk or 'F' was added if the synthesis method was based on IZC (crystalline sources) or on fluoride, respectively (see section S1).

2.2. Activation Protocols

2.2.1. Air Calcination. High-temperature static air calcination was performed in a muffle furnace (P330/B180, Nabertherm) in porcelain plates in a shallow bed configuration, heated at 1°C/min from room temperature to a set temperature (typically 580°C) and then held for 6 h before gradual cooldown. The latter was labeled accordingly 'O_2(temperature)'.

2.2.2. Ozonation. Low-temperature ozone activation was performed in a tubular reactor in a tangential (cross) flow set-up, as depicted in Figure 1. The as-made zeolites are placed in a porcelain disk ('boat') in a shallow bed configuration. The disk is placed in a borosilicate glass tube and inserted in the cylindric reactor. The latter is surrounded by an isothermal heating element (oven) and connected via adequate ozone-resistant tubing (PFTE). A controlled flow of oxygen (>99.5 wt.% O_2, ≤10ppm H_2O) is fed to a commercial ozone generator (Longevity, EXT120). The ozone outlet concentration depends on the adjustable power applied during corona discharge and on the ozone flow (See supporting info, section S2). *Caution: ozone*

exposure is harmful when inhaled and a potential air pollutant. KI scrubbers were used to trap O_3 residues. For the sensitivity analysis, 2x 100mg was added, having the *MFI[40;Na]* benchmark down-flow of the *CHA[15;Na]* benchmark. Ozonations at standard conditions (150°C; 24ml/min; 50µg O3/ml) are labelled 'O_3(ozonation time)'.

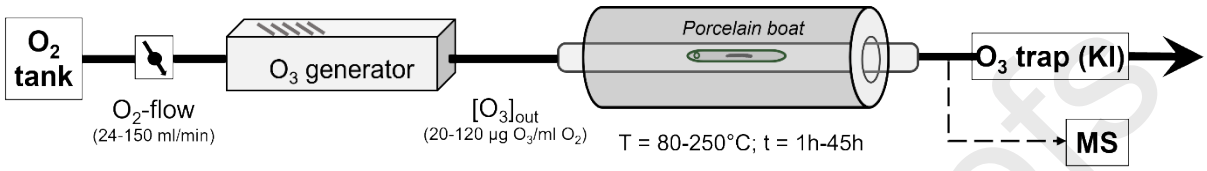

Figure 1: Schematic overview of ozonation set-up. MS is the mass spectrometer.

2.3. Characterization methods

2.3.1. Thermogravimetric analysis (TGA). TGA was performed on as-synthesized and (partially) activated zeolites using a TA Instruments TGA Q500 under an O_2 flow (90ml/min) at heating rates of 10°C/min. Samples were placed on tarred Pt pans. The TGA data were used to quantify the OSDA removal efficiency (η, see section 2.4).

2.3.2. Nitrogen physisorption. Porosity is measured by nitrogen physisorption (Tristar II 3020, micrometrics) at -196°C (77K) on (partially) activated samples. Instead of conventional 300°C pretreatment, prolonged (>8h) pretreatment at 150°C was applied to prevent (additional) temperature-related structural changes. In a compromise, 20-25% lower microporosities were achieved. The relative nitrogen pressure was varied between 0.01 and 0.99 (p/p_0). The t-plot method (Harkins and Jura) on the adsorption branch between 0.2 and 0.4 p/p_0 is used to determine micropore volumes.

2.3.3. CN Analysis. Elemental carbon and nitrogen were determined by an elemental analyzer (EA 1110, CE Instruments) with combustion at 1020°C and reduction at 640°C. A ConFlo IV interface (Thermo Scientific) is used for connection to an IRMS system (Delta V, Thermo Scientific). Elemental fractions are scaled to the overall sample weight.

Journal Pre-proofs

2.3.4. Scanning Electron Microscopy (SEM). Analysis was performed on the Jeol JSM-6010LV microscope at an acceleration voltage of 15kV. Zeolite samples were attached to a piece of carbon tape. Subsequently, a thin Pd/Au (60/40 ratio) layer was deposited on top of samples to achieve sufficient conductivity.

2.3.5. Fourier transform infrared spectroscopy (FT-IR). Vacuum FTIR spectroscopy was performed on KBr wafers containing 1.6 wt.% of zeolites using a Bruker IFS 66 v/S Vacuum FTIR spectrometer (128 scans and resolution 4 cm^{-1}) equipped with a pyroelectric deuterated L-alanine doped triglycine sulfate detector (DlaTGS). The obtained spectra were analysed with the Bruker OPUS software (version 7.5).

2.3.6. Mass spectroscopy (MS). The composition of the effluent gas during template removal of SSZ-13 was analysed by an online quadrupole mass spectrometer (GSD350, Pfeiffer) at constant vacuum pressure ($<10^{-5}$ bar). A broad range of m/z values was collected at 256ms each (m/z = 2, 12, 14, 15, 16, 17, 18, 27, 28, 29, 30, 32, 44, 46, 48). Before testing, effluent tubing was flushed for 20 minutes using ozone and stabilized for 1 hour at 150°C under O_2 to eliminate eventual residues.

2.3.7. Raman Spectroscopy

Raman spectra were measured on a Bruker Vertex 70 spectrometer with RAMII Raman module laser (1064 nm) at a power of 40 mW and accumulating 2048 scans at a resolution of 2 cm^{-1}.

2.4. Defining OSDA removal efficiency

$$OSDA\ removal\ (\%) = \eta_i = \left[1 - \frac{TGA_{\Delta T}(sample\ i) - TGA_{\Delta T}(ref.)}{TGA_{\Delta T}(as-made)}\right] * 100 \quad (eq.\ 1)$$

The OSDA removal efficiency was determined with the TGA weight loss percentages in a particular temperature range of the (ozonated) sample 'i' ($TGA_{\Delta T}(sample\ i)$), the empty air

calcinated version of the sample ($TGA_{\Delta T}(ref.)$), and the as-synthesized zeolite ($TGA_{\Delta T}(as-made)$). Variable ΔT ranges are applied dependent on the OSDA-framework combination. For SSZ-13 (CHA), a range between 350°C-650°C is set, whilst a range between 350°C-550°C is used for ZSM-5 (MFI), or 250°C-650°C for zeolite beta (BEA). $TGA_{\Delta T}(ref.)$ is subtracted to compensate for the inherent minimal weight-loss reported for completely empty zeolites (0-1 wt.%), likely from silanol condensations or other structural healing.[8,10] Quantification of $TGA_{\Delta T}(sample\ i)$ is demonstrated for a variety of *CHA[15;Na]* samples with variable ozonation times (Figure S1). Reproducibility of the TGA experiment is proven in the supporting information (Figure S2) and further evidenced from the high correlation with carbon elemental analysis (see below).

3. Results:

3.1. Quantification of OSDA removal

Several *CHA[15;Na]* with different levels of OSDA removal were fully characterized by TGA, elemental analysis, and nitrogen physisorption and used to validate the quantification of OSDA removal. Figure 2 indicates a very high correlation between the defined removal efficiency parameter (see section 2.4.) and the increase of the microporosity values (blue) and the fraction of removed carbon as measured by CN-analyses (black). Hence, the TGA-based OSDA removal efficiency parameter (η) is a good proxy for both the removal of carbonaceous templates (*detemplation*, although most OSDAs are not to be seen as strict templates) and for the micropore volume becoming available (*emptying*), both for ozonated (figure 2) and air calcined samples (figure S3). The latter was performed in classic air calcinations with different temperatures (300 – 580 °C) to get a series with similar partial removal. An ozone sample with η = 61% has 62% of its original C removed, but only 38% of the N present in the initial as-made material, implicating that elemental N is removed less efficiently than carbon during

(ozone) detemplation. Lower N removal was also found for air calcined samples at 450°C (figure S3) and air calcination literature data.[33]

The 580°C air calcined zeolite (η = 100%, by definition) contains the lowest CN values, close to the detection limit (Figure 2, cross). Completely emptied *CHA[15;Na]* via ozonation are also relatively void of C but still contain 0.89 wt. ‰ of N (Figure 2, triangle), corresponding to 5.6% of the original amount. Structural and textural integrity was asserted from respectively nitrogen physisorption (Figure S4) and SEM images (Figure S5). As demonstrated in Figure 2, micropore volume increases linearly with removal efficiency. Both total pore volumes and micropore volumes are identical after complete template removal ($V_{micr.}$ = 0.27 cm³/g; $V_{tot.}$ = 0.28 cm³/g for *CHA[15;Na]*)). Hence, no noticeable structural degradation was caused by the 'low temperature' removal method.

Journal Pre-proofs

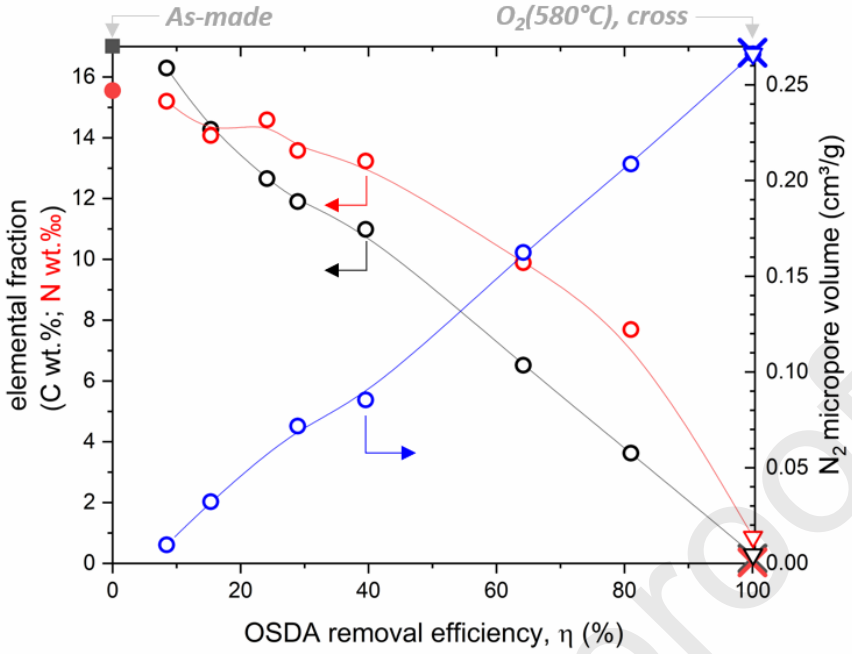

Figure 2: Quantification of OSDA removal efficiency via TGA (x-axis, eq. 1) compared to elemental content of carbon (black, wt.%) and nitrogen (red, wt.‰) on the left y-axis and t-plot microporosity (blue, right y-axis). Data is presented for a *CHA[15;Na]*: as-made (filled symbols), partially emptied via ozonation (open circles; O_3-150°C; 50 µg/ml; 24ml/min, variable time), fully emptied via ozonation (triangle; O_3-175°C; 90 µg/ml; 90ml/min, 24h) and for an air calcined sample (crosses; O_2(580°C)). Figure S3 demonstrates an equivalent (T-based) plot for air calcination.

3.2 Influence of relevant process parameters

Two benchmark samples with different properties were made in the lab (see section 2.1.): ZSM-5 (*MFI[40;Na]*) and SSZ-13 (*CHA[15;Na]*). As the sample position was detected as an influential parameter on OSDA removal (see supporting info, section S3), all analyses in 3.2. were performed on one centered porcelain boat containing twice 100mg, with the *MFI[40;Na]* downflow of *CHA[15;Na]*. The experimental data are summarized in Figure 3. For all the single-parameter variations, it was decided to pivot around standard conditions of 24 ml/min

Journal Pre-proofs

O_2 flow, an ozone concentration of 50 µg per ml O_2 concentrations, an ozonation time of 19h, and an oven at 150°C. At these standard conditions, *MFI[40;Na]* and *CHA[15;Na]* have η = 98% and 72% respectively (black arrows in figure 3).

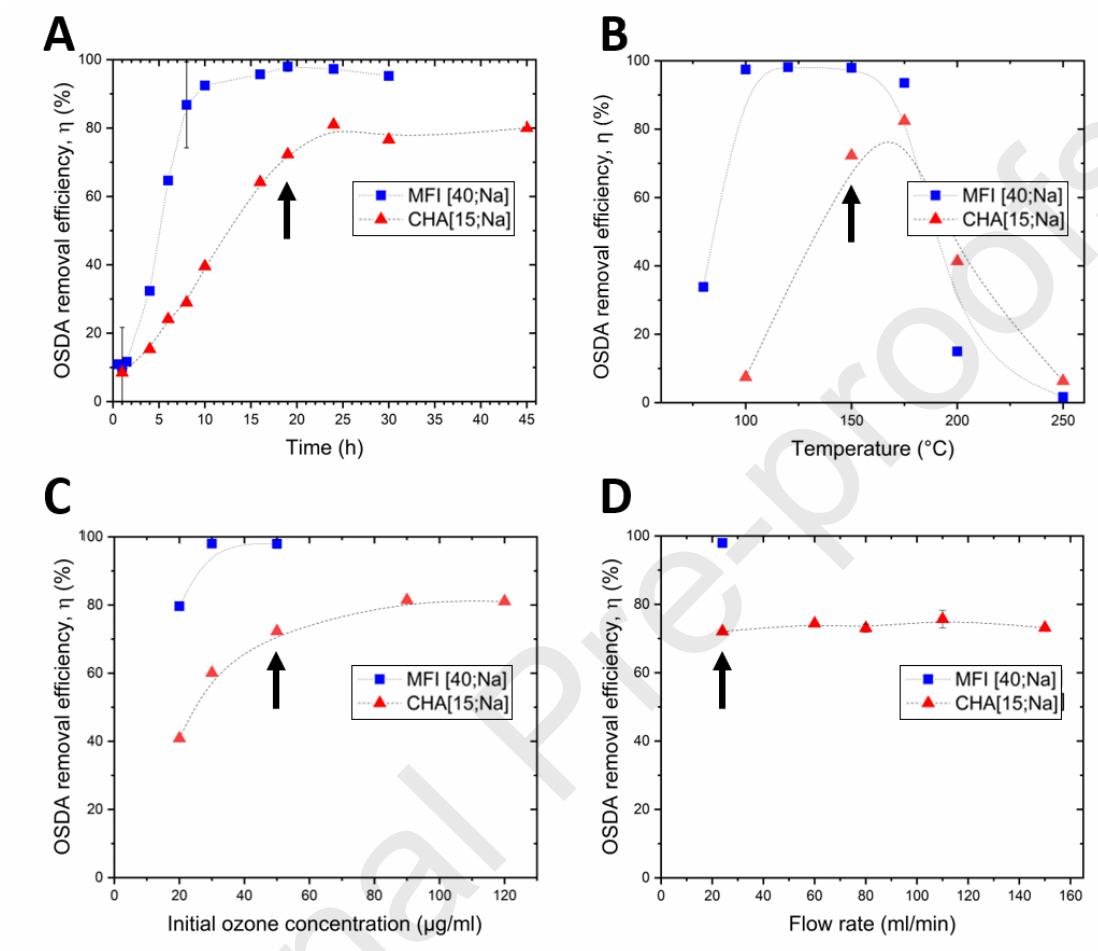

Figure 3: OSDA removal efficiency (η) for benchmark samples (*MFI[40;Na], CHA[15;Na]*) using single-parameter variations pivoting at standard conditions (24 ml/min, 50 µg/ml, 19h at 150°C, black arrow): variation of ozonation time (A), variation of ozonation temperature (B), variation of (initial) ozone concentration (C), and variation of the flow rate (D). Error bars indicate one standard deviation based on identical ozonation runs of the same as-made material.

3.2.1. Influence of time. For the medium-pore sized (10-membered ring, 10MR) *MFI[40;Na]* zeolites, the detemplation is complete within 10h, whilst a significant fraction (~20 wt.%) of OSDA is not removed from *CHA[15;Na]* under standard conditions (Figure 3A). Seemingly,

Journal Pre-proofs

OSDA removal occurs at a constant rate in time. OSDA removal rates of *MFI[40;Na]* are estimated four times higher (η = 16 %/h) than for *CHA[15;Na]*. The slow removal rates for the SSZ-13 (CHA) can be explained in part by its nearly double OSDA content (in weight) versus ZSM-5, as evidenced from TGA. However, other structure-specific factors are also at play.

3.2.2 Influence of temperature. OSDA (template) removal operates in a narrow temperature window (100°C-200°C, Figure 3B). In the more restricted *CHA[15;Na]* case, this temperature window is even smaller and shifted to higher ozonation temperatures. It is also important to note that the oxidation of carbonaceous species is highly exothermic.[34] Hence, internal temperature gradients may also exist, as observed experimentally in an analogous LT activation system (using plasma).[23]

3.2.3. Influence of concentration. Complete ozone removal was possible with only 30 μg O_3/ml for *MFI[40]*, whilst at least 90 μg/ml was required to optimize OSDA removal in *CHA[15;Na]* (Figure 3C). Note that the absolute values are based on the ozone generator data (see Section S2). In contrast to the linear time trend, the OSDA removal is asymptotic with concentration. Seemingly the same 20% that could not be removed with prolonged time (>24h) is also remnant at increased O_3 concentrations, hinting towards a similar (removal) limitation of the system.

3.2.4 Influence of flow rate. CHA[15;Na] was not affected by altering the volumetric flow of the system (Figure 3D). In fact, the OSDA removal limit (η=~80%) is not met. Instead, the dataset validates the reproducibility of the output of the standard condition (η= ~72%, black arrow). Note, however, that flow can be an important parameter in some other CHA synthesis systems (figure S6).

3.2.5 Synergetic parameter optimization. The sensitivity analysis above provides the opportunity to tailor each synthesis-dependent removal process. Detemplation of *MFI[40;Na]* is possible at standard conditions at 150°C and 24ml/min (19h; 30 μg/ml) by either reducing

Journal Pre-proofs

the activation time to 8 hours or reducing O_3 concentrations to 30 µg/ml. Further reducing these values did not yield complete detemplation. In an 8 hour process, nearly 16% of the produced ozone is theoretically calculated to have been required for complete combustion of a (TPA) template (see section S4). In contrast, standard conditions were insufficient to completely empty *CHA[15;Na]*. By adapting a flow rate of at least 60ml/min, and an ozone concentration of 90 µg/ml at 175°C, a complete template removal was achieved reproducibly within 24 hours of ozonation (Figure 2, triangle). Beside condition optimization, an even more significant margin for improvements could come from engineering solutions such as changing the flow set-up to a fixed-bed set-up forcing ozone to contact the zeolite.

From this single-parameter analysis of process parameters, it can be concluded that ozonation is very sensitive to oven temperatures, as only a select operation window exists between 100°C-200°C. However, the required ozone concentrations are remarkably low (>100 µg O_3/ml), and the influence of total gas flow is only minor. Cross-comparison indicates that full OSDA removal of the *CHA[15;Na]* benchmark requires a temperature set at 175°C in synergy with an increase in ozone concentration (and correct flow).

3.3 Influence of relevant zeolite parameters

From the analysis of the processes above, it becomes clear that specific zeolite properties also have a significant influence on ozonation. Figure 4 demonstrates detemplation results for framework-OSDA complexes with different pore sizes (SSZ-13, ZSM-5, and zeolite β in Figure 4A, 4B and Figure 4C resp.), Al contents (Si/Al ratios) and crystal sizes.

3.3.1 Influence of framework-OSDA complex. Generally, OSDA removal is most efficient in the large pore zeolite β (BEA, Figure 4C) and most difficult in the small pore SSZ-13 (CHA, Figure 4A), which suggests pore (or cage) diffusion-limited OSDA removal. Despite similar amounts of charge balancing ions present during synthesis (stoichiometric batch content, see

Table S1), there is also a large difference in removal efficiency for a specific OSDA-framework complex dependent on other synthesis-related factors. OSDA removal (efficiency) is also OSDA-framework and synthesis-specific during conventional oxygen calcination as detected by variable themal behaviour during TGA oxidation (Figure S7-S8).

3.3.2 Influence of Al content. There is a general trend towards higher OSDA removal efficiency with higher Si/Al (Figures 4, greyscales). However, also in this case, there are exceptions to the trend. For example, after standard ozonation treatment of *CHA[X;Na]*, OSDA removal is more complete at Si/Al = 15 than at Si/Al= 40 (Figure 4A).

3.3.3 Influence of particle size. Figure 4A also demonstrates the effect of particle size on the standard ozonation conditions. The vast majority of OSDA is removed from the smallest CHA zeolite. However, no clear trend is found between OSDA removal and crystal sizes. Average crystal sizes were estimated from SEM images (Figure S5). Also, note that increased flow fosters OSDA removal to a variable extent in different CHA systems (Figure S6). No particular correlation with crystal size was found.

3.3.4 Influence of other zeolitic properties. No particular effect of sodium was detected. Sodium is known to influence synthesis as an inorganic structure-directing agent and affects more than just one zeolitic parameter. Other zeolitic properties such as morphology, acid site type, and strength oracid site distributions were not captured.

Overall, the most important zeolitic parameters determinant for OSDA removal are the size of the zeolitic pores and the Al content of the latter. In addition, the crystal size is also a significant determinant. Cross-comparison indicates, however, that it is difficult to predict OSDA removal efficiency, entailing a complex reaction mechanism.

Journal Pre-proofs

3.3.5 Comparison to high-temperature air detemplation. Similar to O_3 detemplation, faster OSDA removal was generally found in larger pore zeolites with lower Al contents and smaller particles (see Figures S6-S7). However, the different peaks of derivative weight loss (DTG) already give away the more complex nature of the OSDA removal.

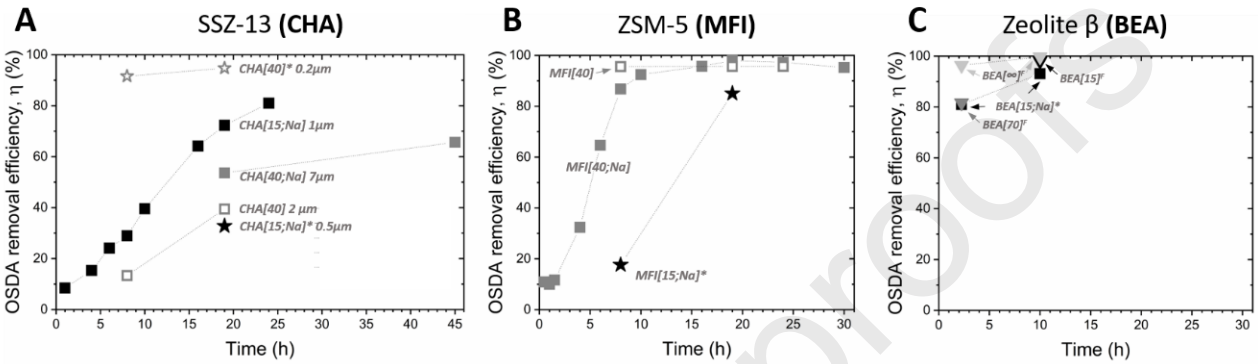

Figure 4: OSDA removal efficiency (η) at standard conditions (24 ml/min, 50 µg/ml, 19h at 150°C) in different OSDA-zeolite systems: in a small-pore **CHA** (A), a medium-pore **MFI** (B), and in a large-pore ***BEA** (C). For each system, a variety of as-made materials (different symbols) with variable properties (Si/Al ratio, synthesis method, crystal size, …) are tested at variable ozonation times. The as-made materials are labeled in the graph (cfr. 2.1.). Average crystal sizes (see figure S5) have been added to the labels in figure 4A.

3.4 Mechanistic investigation

3.4.1. Zeolitic ozone consumption. The behaviour of ozone in the presence of zeolites was quantified by analyzing the effluent gas of ozonation with online mass spectrometry (as shown in the scheme of Figure 1). Under standard conditions, steady-state ozone concentrations were found at 150°C and 175°C for samples with a different extent of OSDA removal (Table 1). Two elements stand out. Foremost, the ozone concentration decreases 6-10 times by increasing the oven temperature. This is caused by thermal ozone destruction due to the decrease of the half-life of ozone to values on the same time scale as the gas retention time of the system (see section S5). Such dramatic O_3 decreases were also observed by Kuhn et al. within a similar

temperature range.[15] Secondly, ozone consumption increases with OSDA removal (increased η). From the latter, it can be deduced that micropores participate in the adsorption and destruction of ozone, which is a bit surprising given its relatively larger molecular (static) diameter (4.62 Å)[15,35] in comparison to the 8MR aperture of CHA (3.72 Å).[32]

Table 1: Steady-state MS intensities of ozone (m/z=48) linked to destruction on (partially emptied) CHA[15;Na].

CHA[15;Na]	**η (%)[c]**	MS intensity (10^{-10})	
		150°C	**175°C**
No sample	N.A.	7.4	1.7
As-made	0	6.4	1.1
End of MS cycle[a]	95	2.3	/
Empty by ozonation[b]	100	2.1	0.2

[a] procedure see below in 3.4.2[b] after ozonation (60ml/min and 90 µg O_3/ml for 24h at 175°C); [c] ozone removal efficiency as defined in 2.4.

3.4.2. Comparison between oxidation atmospheres. Online mass spectrometry was performed on as-made zeolites studying the outlet flow in ozone-containing or pure oxygen detemplation regimes. *CHA[15;Na]* (100 mg; η = 0) was loaded, heated to 150°C, and subjected to standard (24 ml/min, 50 µg O_3/ml) ozonation for 2 hours, including an intermezzo at 175°C (Figure 5A). Next, the sample is heated under pure oxygen to 450°C (at 5°C/min, with a plateau at 350°C and 400°C) and gradually cooled (Figure 5B) under identical flow conditions (24 ml/min, 0 µg O_3/ml). It is anticipated that the relatively short ozonation procedure preceding the O_2 procedure will have a limited impact on the latter, allowing direct comparison of two activation atmospheres (LT-O_3 and HT-O_2), due to the limited OSDA removal efficiency (η) of just 10-15% predicted for the first O_3 step (based on the parameter analysis of 3.2).

Journal Pre-proofs

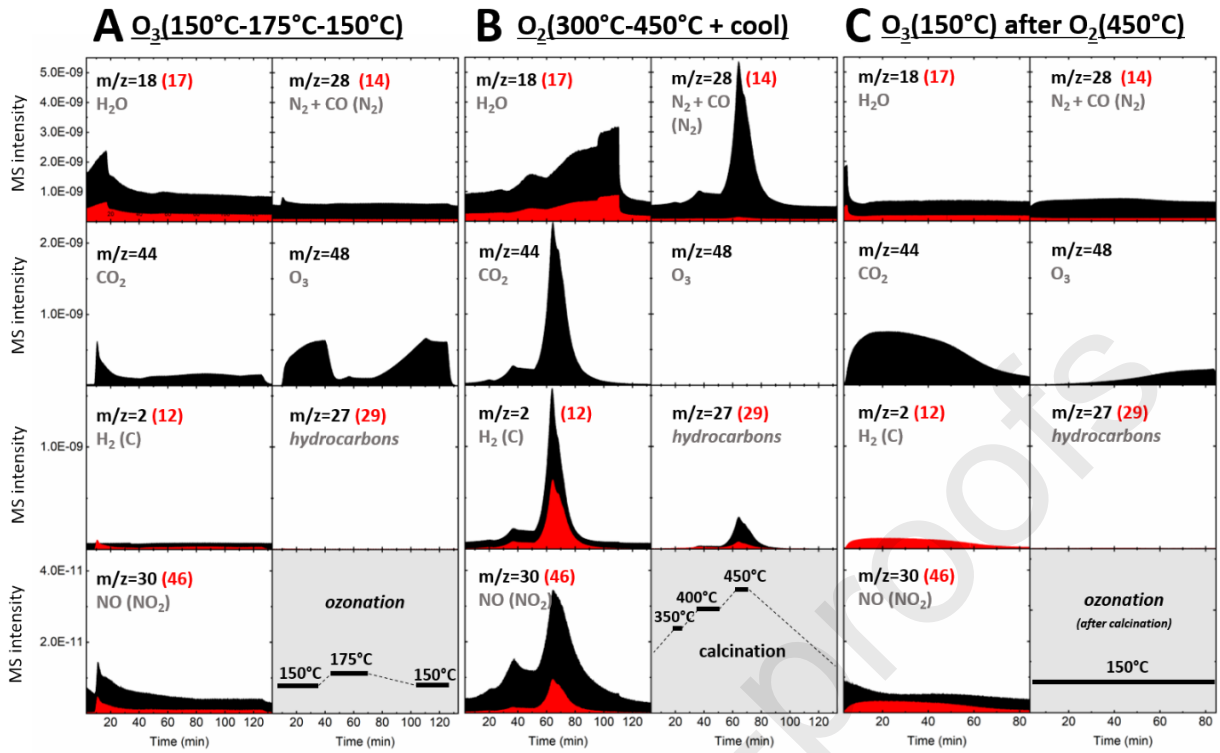

Figure 5: MS spectra outlet of SSZ-13 (*CHA[15;Na]*) activation during three consecutive procedures: (A) standard ozonation at 150°C and 175°C (see grey box). (B) high-temperature O_2 calcination in a temperature range of 300°C-450°C (5°C/min heating ramp). (C) LT ozonation standard calcination at 150°C (after O_2). The y-axes scales are identical in each row. Contributions for oxygen carrier gas (m/z = 32;16;8) and residual argon (m/z = 40) are not shown. Mass exploration (m/z = 1-70) did not shown other significant contributions. The molecule attributing (mainly) to the m/z values are assigned in grey. Red signals have their m/z values (red) and its molecular assignment (grey) between brackets.

Figure 5 demonstrates MS results for the most significant m/z values, omitting the dominant m/z = 32 and m/z = 16 signals from the O_2 carrier gas. In the first minutes of ozonation (figure 5A) small spikes were detected for CO_2 (m/z = 44), H_2O (m/z = 17, 18), and to a lesser extent for C^+ (m/z = 12) and NO_x species (m/z = 30, 46). After this, O_3 contributions (m/z = 48) gradually increase, and after ~40 minutes, an equilibrium is reached with relatively high O_3 concentrations at 150°C (m/z_{48}= 6.4 10^{-10}, see table 1). In contrast to the thermal effect on

ozone concentrations (3.4.1), other MS signals remained relatively constant upon temperature increase to 175°C. Only a minor increase in CO_2 (m/z_{44}) and C^+ (m/z_{12}) was observed, indicating a rather limited increase in detemplation rates (figure 5A). From the latter, it can be hypothesized that ozone-based template removal is a slow steady-state process with mainly formation of combustion products (CO_2). In contrast, high-temperature detemplation spikes thus occur much faster and also generate a significant amount of hydrocarbonaceous exhausts (m/z= 15, 27, 28, 29) or potentially alkylamines (m/z=30) next to H_2O, CO_2, and H_2 (Figure 5B). These species are typical for β-eliminations (Hofmann) and incomplete oxidation.[36–38]

3.4.3. Alternating atmosphere procedures (O_2-O_3). Zeolites were switched from the activation method at intermediate degrees of OSDA removal. Zeolite powder after partial ozonation turned from white to yellowish-brown after an additional high-temperature treatment (O_3(6h) + O_2(450°C)). The inverse occurred upon ozonation of (partially) air calcined samples (O_2(450°C) + O_3(1h)). These atmosphere-specific colour changes were not only detected for SSZ-13 (*CHA[15;Na]*), but also for ZSM-5 (*MFI[40;Na]*), and are an indication of coke residues on the zeolitic surface during conventional (high temperature) detemplation.[37,39] Figure 6 demonstrates the elemental removal efficiency calculated for carbon and nitrogen. While detemplation at 450°C was much more advanced than after 6 hours of ozonation, additional OSDA removal after 450°C using ozone was surprisingly efficient (O_2(450°C) + O_3(1h)). 99% of C was removed within one hour, and the colour disappeared (Figure S9). In contrast, very little N was removed during the additional hour of ozone. The O_2-O_3 detemplation sequence was also investigated by MS performing ozonation at standard conditions (150°C) after the 450°C (see 3.4.2). Figure 5C suggests very abundant oxidation to CO_2 (m/z_{44}; m/z_{12}) and no formation of hydrocarbonaceous species ($m/z_{27\text{-}30}$). The latter backs the observation of fast carbon removal and reconfirming the different nature of detemplation atmospheres and processes. During the initial 40 minutes, ozone presence was very limited,

most likely due to extensive C oxidation. After ~80min, equilibrium ozone contributions were established, and the zeolite was nearly empty (η = 95%, see Table 1 'end of MS cycle').

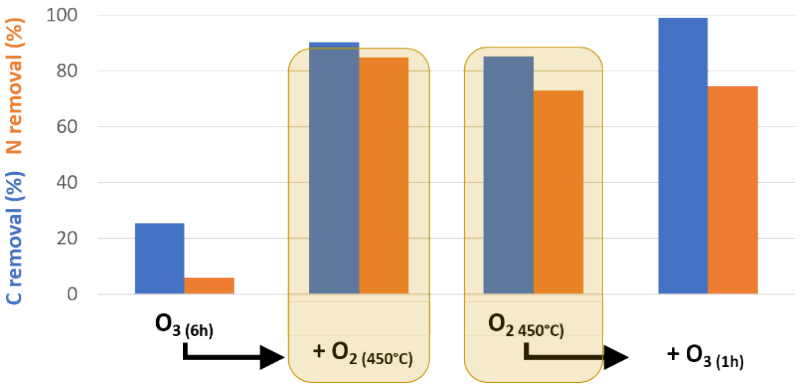

Figure 6: Elemental C (blue) and N (orange) removal efficiency (scaled against the CN content of as-made materials) for different activation treatments on a *CHA[15;Na]* benchmark synthesis. Labels indicate the oxidation environment (O_2, O_3, or a sequence thereof). The arrow indicates that a second treatment is performed consecutively on the specific sample. An orange background depicts the presence of colour after the specific treatment (see figure S9). The hybrid sequence on the right (O_2/O_3) offers an effective low(er) temperature route (4.2).

3.4.4. Intact organics at partial oxidation conditions. Samples with different activation environments were subjected to FTIR and Raman spectroscopy to understand the nature of OSDA decomposition (Figure 7). C-H stretching bands (2850-2950cm^{-1}) and vibration bands (1400-1500cm^{-1}) were observed in the as-made materials in addition to a small band at the 3045cm^{-1} characteristic of the N-H stretching (Figure 7A). These bands gradually decrease with the increase of the ozone activation time. However, the C-H and N-H bands signatures were largely maintained, indicating the presence of a large residual fraction of entrapped OSDA (trimethyladamantylammonium) within the zeolite. The results were very different in the case of air-calcined samples (450°C), since only a minor signal of the OSDA bands (2850-

3050 cm^{-1}) was present, despite just 85 % OSDA carbon removal. By quantification of the vibrational band (2850-3050 cm^{-1}), the O_2(450°C) sample showed just 5% of the peak area in as-made materials whilst an ozonated sample with similar carbon removal (O_3(24h); η = 81) has 20% of the peak area in as-made materials, so proportional to OSDA removal (η). Raman spectroscopy, captured at low beam strength (40mW) to prevent coke dissociation, confirms the presence of cokes characterized by broad peaks situated around 1500 cm^{-1} in calcined samples (Figure 7B) whilst such features are largely absent in ozonated samples (Figure 7C). In the latter case, typical Raman signatures for the OSDA (TMAda) are detected (compare to Figure S10).

Hence, both FT-IR and Raman spectroscopy are a good indicator for the structural decomposition of the OSDA at elevated temperatures (400-450°C) in air (cfr. [36]) and OSDA intactness during low-temperature ozonation and this corroborates that different factors are at stake dependent on the activation atmospheres. Furthermore, the intactness of OSDA is also suggested from thermogravimetric results as the temperature of maximum OSDA weight loss was not shifting to higher temperatures upon progressive OSDA removal (Figure S1).

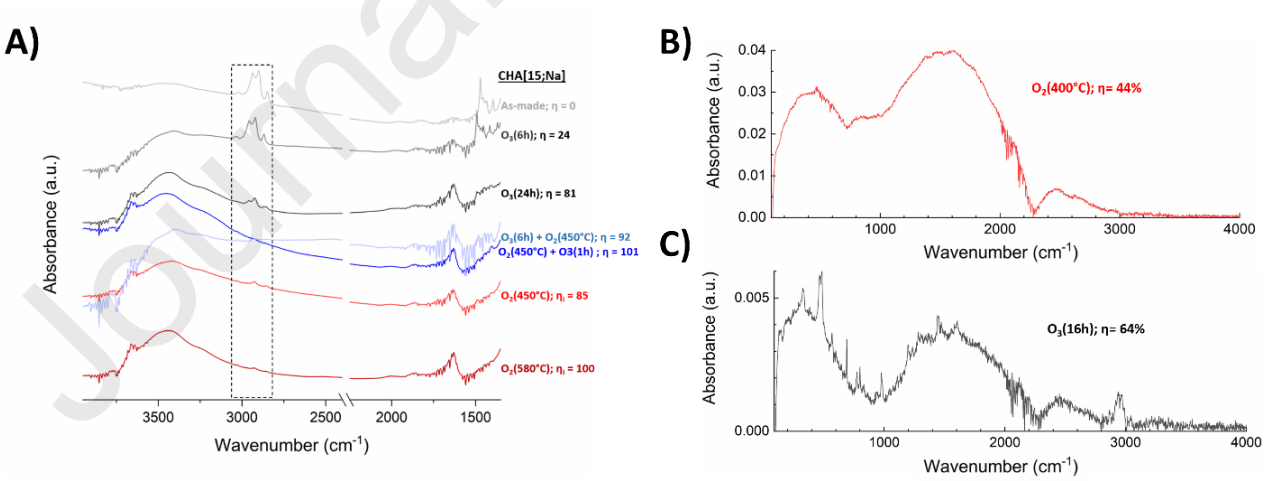

Figure 7: Spectra of (partially) activated SSZ-13 (*CHA[15;Na]*). Labels indicate the oxidation environment (O_2, O_3, and sequences thereof) and OSDA removal efficiency (η). A) FT-IR under different template removal conditions. The OSDA stretching band region is marked

(2850-3050 cm^{-1}). Peaks related to ambient CO_2 (2250-2400 cm^{-1}) are omitted. B) Raman spectroscopy of a partially oven-calcined sample C) Raman spectroscopy of a partially ozonated sample (lower intensity than B).

4. Discussion:

4.1. Mechanism of OSDA removal during ozonation

The vast dataset (>95 ozonation experiments; 12 as-made zeolites) suggests that ozonation is most limited by the size of the pore. Large pore *BEA zeolites are easy to activate, and medium pore MFI can be emptied at 100°C, indicating limited diffusion limitations or ozone degradation. However, in the case of small pore CHA, more severe limitations exist, especially at the lower temperature window and at lower ozone concentrations. Ozone removal (in *CHA[15;Na]*) is only complete at much higher ozone concentrations in the flow and at increased temperatures of 175°C.

For both CHA and MFI benchmarks, relatively constant removal efficiency rates are observed at standard conditions (3.2., figure 3A). Hence, it seems that the removal rates are independent of the OSDA concentration, which can be explained by a layer-by-layer removal (or a shrinking core process, cfr. Levenspiel[40]), where access to the OSDA is hindered by other organics closer to the surface. The latter behaviour is also observed during coke removal treatments using ozone[41] and is also corroborated from the OSDA intactness suggested from the FTIR and Raman results (3.4.4.). Ozone concentrations may decrease with slow intrapore diffusion towards the more internal (not yet removed) OSDA. We cannot predict the extent of ozone depletion with distance to the encaged OSDA. A lot of data on the small pore zeolite (*CHA[15;Na]*) corroborates severe depletion with distance. MS results indicate that (catalytic) ozone degradation occurs more extensive when zeolite emptiness increases and process parameter investigations (at standard conditions) suggest a severe form of ozone depletion with

distance, even to 0, as a final OSDA fraction (~20%; plateau level at η = 80%, figure 3) cannot be removed by increasing either OSDA concentrations or time (figure 3).

Slow diffusion through the material has also been used as an explanation for the observation of linear removal rates in a shrinking core model in other (diffusion-limited) systems,[42] backing the fact that detemplation likely occurs according to a shrinking core model (at least for CHA zeolites). Varying diffusion (and thus also ozone destruction) is expected on the way towards the remnant fraction, and mainly dependent on the pore size (Knudsen diffusion) and perhaps also on the nature of the surface (H_2O, C-remnants, Al-content). The molecular (static) diameter (4.62 Å)[15,35] of ozone is within the range of zeolitic pore sizes. Unfortunately, the kinetic diameters of ozone are not published in the open literature to the best of our knowledge. A large diffusion limitation is expected for small pore zeolites ($8MR_{CHA}$ = 3.72 Å)[32], while a significant but smaller diffusion contribution is expected in medium pore materials ($10MR_{MFI}$ = 4.5 Å)[32], as observed from faster rates. No (or minimal) diffusion is expected in large pore zeolites ($12MR_{*BEA}$ = 5.95 Å).[32] Much faster ozonation during removal of OSDA that is impregnated on mesoporous silica (MCM-41) further confirms the pore size diffusion trend (see figure S11). Next to pore size, other factors such as the crystal size and Al content may also influence intrapore diffusion of ozone and thereby (catalytic) degradation. Note for example the low concentration of ozone in the exit stream (Table 1, MS) when an emptied CHA zeolite with its large internal surface is allowed to interact with the ozone flow, catalytically destroying a lot of ozone (78% less ozone in the exit versus an empty tube experiment). This may explain why ozone activation tendencies are much more related to the material properties, and thus seemingly more variable, in CHA than in MFI or *BEA zeolites (figure 4 and Figure S6).

No or limited ozone gradients are expected at standard conditions within these larger pore materials. Sufficient ozone should reach the OSDA molecules (MFI can be fully emptied at 30

Journal Pre-proofs

μg O_3/ml). The first OSDA degradation step is suspected to be the rate-limiting step rather than degradation products having diffusion limitations. Oxidation of alkanes using ozone (ozonolysis) is believed to be relatively limited (the activation energies for ethane and propane are in the range of 60 kJ/mol[43] versus ~22 kJ/mol[44] for ethylene). If the (initial) OSDA breakdown step is rate-limiting, it can be expected that OSDA removal occurs fastest in the small pore SSZ-13 (CHA) than in the ZSM-5 (MFI) case due to the susceptibility of the more polar and branched compounds. Trimethyladamantylamonium (used for CHA) is asymmetric, its OSDA is less shielded (polar), and it contains tertiary carbons, which are known to be more susceptible to ozonolysis than primary carbons.[45] In contrast, tetrapropylammonium (used for ZSM-5) is less polar (more shielded) and contains no tertiary carbons. This may explain why ozonolysis is more successful in CHA than in MFI at 200°C (figure 3B, although it should be noted that only two samples with different Al contents are compared). It is expected that (thermal) O_3 degradation occurs to the same extent when diffusion becomes less of an issue (e.g., 200 °C), allowing the effect of intrinsic reaction rates of ozone with the organic to dominate.

Despite the collected data, it was not possible to pinpoint a precise and generic mechanism predicting the variety of observed trends. Other factors that may also have an influence on ozonation to an unknown extent are:

- The high exothermicity of ozone oxidation.[41,44] The latter may cause local heating (thermal), but no thermal run-off is expected as ozone (initiators) will be thermally depleted. On the other hand, (local) heating towards temperatures above 250°C may induce the (endothermic) Hofmann decomposition. In the case of quaternary ammonium-based OSDAs, the breakdown products (alkenes and tertiary amines) will be very susceptible to ozonation.[45–47] (see below).

Journal Pre-proofs

- The nature of the radical induced oxidation mechanism. OSDA removal may be induced by an indirect oxidation of hydroxyl radical intermediates instead of direct ozone oxidation.[48,49] These are much smaller (2.64 Å) and a stronger oxidant (E° = 2.7eV) than ozone (E° = 2.1eV). The ozonation study of Zhang et al. suggests this pathway, as a link is demonstrated between faster detemplation and water present in the carrier gas.[18] An OH° induced pathway is likely, especially due to the fact that water is abundantly present in zeolites within the typical temperature window of ozonation (<200°C),[10] but (long-range) diffusion of the species is questionable given its very short lifetimes.[26] Nonetheless, it cannot be excluded that (ozone) diffusion limitations reflect, in fact, the concentration of (hydroxyl) radicals rather than ozone itself.
- The role water has on ozonation is ambiguous. Among others, water can have an influence on the detemplation mechanism (O_3 decomposition to OH° or on Hofmann degradation[50]), on the reaction chemistry (it is a product), on diffusion, on heat dissipation, and on competitive sorption on acid sites (of which some destruct ozone), …

Given the above summation of remaining uncertainties, further investigations are required to expose the (complex) mechanism of ozonation. Especially quantification of deconvoluted activation energies (of OSDA removal) and ozone diffusion constants for zeolites with variable pore size and crystal sizes (among others) would be very informative (but hard to access).

In summary, our data suggest that the initial (first) OSDA degradation step can be rate-limiting during ozonation, but that diffusion plays an important role in a zeolite with small pore sizes. The (radical-based) ozone oxidation is also severely limited at 200°C and above temperatures due to increasing thermal and catalytic degradation of ozone. Taken altogether, our extensive study has allowed establishing some boundary and minimal conditions required

Journal Pre-proofs

for successful ozonation at relatively high efficiency for a large variety of OSDA-framework systems.

4.2. Air calcination and ozone combination methods

Note that ozonation is relatively slow in comparison to high-temperature oxidation (3.4.2.). In the section above, we have argumented that the slow nature of ozonation can be related to the relatively high activation energies for alkanes, diffusion constraints, and thermal ozone degradation at Hofmann degradation temperatures. In contrast, calcination at high temperatures (400-600°C) is rate limited due to limited (O_2) combustion hampering removal of (mass-transfer limiting) cokes formed on the zeolite surface.

According to literature, several removal steps occur during conventional (high temperature) detemplation, limited at different temperature ranges and depending on specific acid sites. Gao *et al.* suggest a limited extent of radical-type TPA^+ decomposition occurs on surface Lewis acid sites at 200-220°C.[38] However, these sites may be quickly covered with cokes. At slightly higher temperatures (still below 300°C), bulk detemplation starts via a Hofmann type degradation facilitated by Bronsted acid sites or defects ($\equiv$Si-O^-).[36,51] During product pore diffusion, the Hofmann degradation products (alkenes and amines) may interact with the encountered acid sites and undergo additional reactions (oligomerization, addition, cyclization, and hydrogen transfer), yielding chained alkanes and larger aromatic products (ultimately cokes).[36,37,39] These products require high temperatures for diffusion and will strongly bind to acid sites on the external surface, causing severe mass-transfer limitations. Removal of the latter (coloured) deposits occurs at the highest temperatures.[51,52] In oxygen-containing media, combustion will lower activation energies (temperature) for complete detemplation.[34,38,51,52] Oxidation was not complete at 450°C in our high-temperature MS test as hydrocarbon species were observed despite the pure O_2 flow (Figure 5B). In contrast,

only oxidation products were observed in ozonated zeolites (Figure 5A), indicating rapid and complete combustion in the presence of ozone. Mimicking the hybrid (O_2/O_3) method by performing (standard) ozonation after 450°C (O_2) calcination (Figure 5C), ozone was absent (initially) in the effluent during this high fast detemplation step. The reactivity of ozone towards the acid-site induced (coloured, figure 6) degradation products stuck on the surface after incomplete high-temperature detemplation can explain the rapid nature of (low temperature) ozonation performed after (incomplete) high-temperature detemplation because ozone is highly selective for the electron-rich amines and unsaturated compounds.[45–47]

Thus, the efficient combination method (3.4.3.) involving ozone after a (short) treatment at dehydrating conditions (e.g., 450°C) proves a way around the bottlenecks of ozonation (temperature-induced Hofmann degradation overcomes initial OSDA breakdown) and of air calcination (ozone depletes cokes). The latter is summarized in scheme 1.

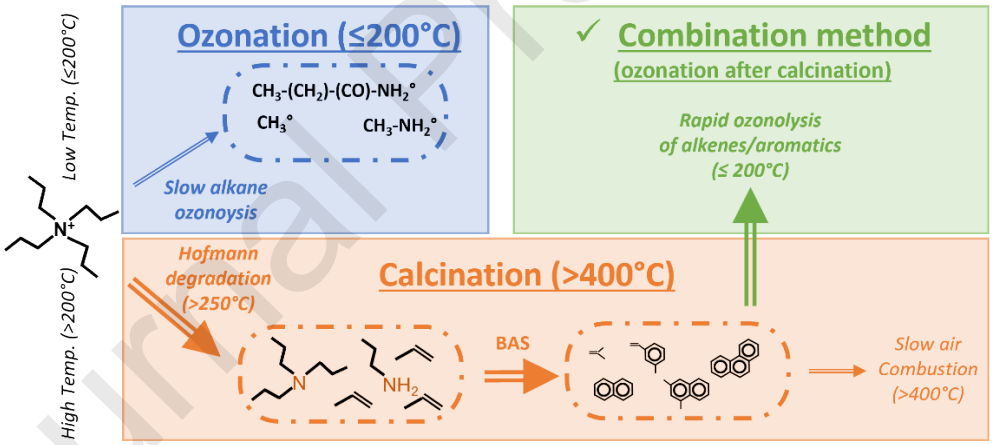

Scheme 1: Visualization of the processes and intermediates during low-temperature ozonation (blue) and higher temperature calcination (orange) and the efficient combination method (green). The bottlenecks of ozonation (initial OSDA destruction) and high-temperature calcinations (combustion of cokes) are indicated by small arrows.

Combined O_2-O_3 detemplation treatments are thus a very promising method to tackle mass-transfer limitations related to surface coke deposits and allow detemplation of zeolites at lower

temperatures (450°C+150°C vs. classic calcination at 550-580 °C). Note, however, that this O_2-O_3 hybrid technique is not very efficient for the removal of N-compounds (Figure 6). Primary alkylamines and ammonia are less susceptible towards ozonolysis.[53] However, the small amount of nitrogen present in OSDAs (C/N = 8-12) is not expected to create the severe mass-transfer limitations encountered due to carbonaceous deposits in conventional high temperature (air) calcinations. Sustained N inclusion may even be desired regarding (NH_4-) exchange properties.

5. Conclusion and perspectives

Encaged templates (more correctly called organic structure-directing agents or OSDAs) were removed from zeolites using a low-temperature process with flowing ozone. Ozonation was optimized for a variety of OSDA-zeolite composites with different pore sizes (SSZ-13, ZSM-5, zeolite β) and a variety of physicochemical properties (Al content, particle size, alkali, …). Without porosity loss or textural deterioration, complete removal on this variety of synthesis-made zeolites was achieved by engineering process parameters such as time, temperature, ozone concentration, and flow rates. From the analysis, it is suggested that the initial (first) OSDA degradation step can be rate-limiting during ozonation and that diffusion can take a dominant role, especially in small pore zeolites. Furthermore, combining high-temperature calcination with low-temperature ozonation made it possible to develop a more efficient combination method, circumventing the bottlenecks of both reactions, namely limited OSDA decomposition at low and cokes formation at higher temperatures.

Additional ameliorations of the ozone efficiency, defined for instance as the percentage of generated ozone actually used for detemplation versus the overall flow are certainly feasible from an engineering point of view (e.g., in a packed bed set-up). This, on top of a reduction of NOx/NO_2 emissions (co-feeding NH_3 and ozone has the potential to accelerate NO_2 destruction

via 'fast SCR' pathways on zeolites. [54]) could make low-temperature ozonation a promising 'low energy cost' process for OSDA removal with reduced environmental impact. Moreover, it can be rationalized that ozone activation has some benefits (e.g., avoiding high-temperature effects) for overall zeolite acidity or hydrophilicity, especially for large-scale calcinations.[38] Future work should investigate the application potential of ozonation, especially in a context where zeolite catalysts are applied in low-temperature catalytic processes (e.g., selective conversion of methanol to dimethyl ether below 180°C[55]). The use of ozone to regenerate coked-up or deactivated catalysts at a low temperature is definitely also an interesting avenue.

6. Appendices

Supporting information is provided (PDF) containing additional characterization: TGA profiles, nitrogen sorption isotherms, Raman spectroscopy, SEM-images, the dependence of ozone removal on flow (in CHA), and sections discussing details on the synthesis method, deduction of (initial) ozone concentrations, the influence of sample position, comments on residence time and thermal ozone destruction and estimations of ozone removal efficiencies.

AUTHOR INFORMATION

Author Contributions

J.D., R.B., S.R., and M.D. designed the research. J.D., R.B., and G.I performed experiments. All authors analysed the data. J.D. wrote the manuscript with the critical input of all authors.

Funding Sources

J.D., S.R., I.K., G.I. and M.D. thank the Research Foundation—Flanders (FWO Vlaanderen) for funding (Grants G0C1618N and G085220N to M.D. and 1260321N to I.K.). J.D. also acknowledges KU Leuven for a PDM grant (3E210695).

Journal Pre-proofs

Notes

The authors declare no competing financial interests.

ACKNOWLEDGMENT

SACHEM is explicitly thanked for providing the organic structure-directing agents (TMAda-OH and TPA-OH). Prof. Dirk De Vos is acknowledged for providing insights on hydrocarbon chemistry with ozone. Dr. Max L. Bols and Dr. Carlos Marquez are thanked for their practical support for mass spectroscopy and FTIR, respectively.

REFERENCES

[1] J. Čejka, G. Centi, J. Perez-Pariente, W.J. Roth, Zeolite-based materials for novel catalytic applications: Opportunities, perspectives and open problems, in: Catal. Today, Elsevier, 2012: pp. 2–15. https://doi.org/10.1016/j.cattod.2011.10.006.

[2] W. Vermeiren, J.P. Gilson, Impact of zeolites on the petroleum and petrochemical industry, Top. Catal. 52 (2009) 1131–1161. https://doi.org/10.1007/s11244-009-9271-8.

[3] A. Palčić, F.Z. Abellán, A. Vicente, C. Fernandez, V. Georgieva, J. Bronić, V. Valtchev, Formation mechanism of three-membered ring containing microporous zincosilicate RUB-17, CrystEngComm. 17 (2015) 7063–7069. https://doi.org/10.1039/c5ce01394a.

[4] C. Röhrig, H. Gies, A New Zincosilicate Zeolite with Nine-Ring Channels, Angew. Chemie Int. Ed. English. 34 (1995) 63–65. https://doi.org/10.1002/anie.199500631.

[5] M. Ravi, V.L. Sushkevich, J.A. van Bokhoven, Towards a better understanding of Lewis acidic aluminium in zeolites, Nat. Mater. 19 (2020) 1047–1056. https://doi.org/10.1038/s41563-020-0751-3.

[6] M. Ravi, V.L. Sushkevich, J.A. van Bokhoven, On the location of Lewis acidic aluminum in zeolite mordenite and the role of framework-associated aluminum in mediating the switch

Journal Pre-proofs

between Brønsted and Lewis acidity, Chem. Sci. 12 (2021) 4094–4103. https://doi.org/10.1039/d0sc06130a.

[7] L. Lang, S. Zhao, J. Jiang, W. Yang, X. Yin, Microporous and Mesoporous Materials Importance of hydrogen for low-temperature detemplation of high- silica MFI zeolite crystals, Microporous Mesoporous Mater. 235 (2016) 143–150. https://doi.org/10.1016/j.micromeso.2016.07.044.

[8] M.J. Ortiz-Iniesta, I. Melián-Cabrera, Fenton chemistry-based detemplation of an industrially relevant microcrystalline beta zeolite. Optimization and scaling-up studies, Microporous Mesoporous Mater. 206 (2015) 58–66. https://doi.org/10.1016/j.micromeso.2014.12.019.

[9] J. Patarin, Mild methods for removing organic templates from inorganic host materials, Angew. Chemie - Int. Ed. 43 (2004) 3878–3880. https://doi.org/10.1002/anie.200301740.

[10] V. Valtchev, G. Majano, S. Mintova, J. Pérez-Ramírez, Tailored crystalline microporous materials by post-synthesis modification, Chem. Soc. Rev. 42 (2013) 263–290. https://doi.org/10.1039/c2cs35196j.

[11] I. Melián-Cabrera, F. Kapteijn, J.A. Moulijn, Room temperature detemplation of zeolites through H2O 2-mediated oxidation, Chem. Commun. (2005) 2744–2746. https://doi.org/10.1039/b502167g.

[12] A.N. Parikh, A. Navrotsky, Q. Li, C.K. Yee, M.L. Amweg, A. Corma, Non-thermal calcination by ultraviolet irradiation in the synthesis of microporous materials, Microporous Mesoporous Mater. 76 (2004) 17–22. https://doi.org/10.1016/j.micromeso.2004.07.032.

[13] Q. Li, M.L. Amweg, C.K. Yee, A. Navrotsky, A.N. Parikh, Photochemical template removal and spatial patterning of zeolite MFI thin films using UV/ozone treatment, Microporous Mesoporous Mater. 87 (2005) 45–51. https://doi.org/10.1016/j.micromeso.2005.07.048.

[14] S. Yang, Y.H. Kwon, D.Y. Koh, B. Min, Y. Liu, S. Nair, Highly Selective SSZ-13 Zeolite Hollow

Journal Pre-proofs

Fiber Membranes by Ultraviolet Activation at Near-Ambient Temperature, ChemNanoMat. 5 (2019) 61–67. https://doi.org/10.1002/cnma.201800272.

[15] J. Kuhn, J. Gascon, J. Gross, F. Kapteijn, Detemplation of DDR type zeolites by ozonication, Microporous Mesoporous Mater. 120 (2009) 12–18. https://doi.org/10.1016/j.micromeso.2008.09.018.

[16] J. Kuhn, M. Motegh, J. Gross, F. Kapteijn, Microporous and Mesoporous Materials Detemplation of [B] MFI zeolite crystals by ozonication, Microporous Mesoporous Mater. 120 (2009) 35–38. https://doi.org/10.1016/j.micromeso.2008.08.061.

[17] S. Heng, P.P.S. Lau, K.L. Yeung, M. Djafer, J.C. Schrotter, Low-temperature ozone treatment for organic template removal from zeolite membrane, J. Memb. Sci. 243 (2004) 69–78. https://doi.org/10.1016/j.memsci.2004.05.025.

[18] Y. Zhang, M. Wang, S. Liu, M. Wang, N. Xu, L. Gao, Separation and Puri fi cation Technology Mild template removal of SAPO-34 zeolite membranes in wet ozone environment, 228 (2019). https://doi.org/10.1016/j.seppur.2019.115758.

[19] L. Wang, C. Zhang, X. Gao, L. Peng, J. Jiang, X. Gu, Preparation of defect-free DDR zeolite membranes by eliminating template with ozone at low temperature, J. Memb. Sci. 539 (2017) 152–160. https://doi.org/10.1016/j.memsci.2017.06.004.

[20] T.L.M. Maesen, H.W. Kouwenhoven, H. Van Bekkum, B. Sulikowski, J. Klinowski, Template removal from molecular sieves by low-temperature plasma calcination, J. Chem. Soc. Faraday Trans. 86 (1990) 3967–3970. https://doi.org/10.1039/FT9908603967.

[21] V. Medvecká, D. Kováčik, A. Zahoranová, M. Stupavská, M. Černák, Atmospheric pressure plasma assisted calcination of organometallic fibers, Mater. Lett. 162 (2016) 79–82. https://doi.org/10.1016/j.matlet.2015.09.109.

[22] Y. Liu, Y.X. Pan, P. Kuai, C.J. Liu, Template removal from ZSM-5 zeolite using dielectric-barrier

Journal Pre-proofs

discharge plasma, Catal. Letters. 135 (2010) 241–245. https://doi.org/10.1007/s10562-010-0290-7.

[23] Y. Liu, Z. Wang, C.J. Liu, Mechanism of template removal for the synthesis of molecular sieves using dielectric barrier discharge, Catal. Today. 256 (2015) 137–141. https://doi.org/10.1016/j.cattod.2015.03.009.

[24] P.T. Ngo, P.N.X. Vo, L.P. Trinh-Le, D.T. Pham, P.D. Phan, C. V. Cao, T. V. Tran, T.N. Luong, Q.L.M. Ha, N. Le-Phuc, Role of e-beam irradiation treatment on detemplation and structural hierarchy of ZSM-5 zeolite, Microporous Mesoporous Mater. 315 (2021) 110928. https://doi.org/10.1016/j.micromeso.2021.110928.

[25] M. Dusselier, J.H. Kang, D. Xie, M.E. Davis, CIT-9: A Fault-Free Gmelinite Zeolite, Angew. Chemie Int. Ed. 56 (2017) 13475–13478. https://doi.org/10.1002/anie.201707452.

[26] A. Paulenova, Physical and chemical properties of actinides in nuclear fuel reprocessing, in: Adv. Sep. Tech. Nucl. Fuel Reprocess. Radioact. Waste Treat., Elsevier Inc., 2011: pp. 23–57. https://doi.org/10.1533/9780857092274.1.23.

[27] P. Monneyron, S. Mathé, M.H. Manero, J.N. Foussard, Regenaration of high silica zeolites via advanced oxidation processes - A preliminary study about adsorbent reactivity toward ozone, Chem. Eng. Res. Des. 81 (2003) 1193–1198. https://doi.org/10.1205/026387603770866371.

[28] L. Yan, J. Bing, H. Wu, The behavior of ozone on different iron oxides surface sites in water, Sci. Rep. 9 (2019) 1–10. https://doi.org/10.1038/s41598-019-50910-w.

[29] J. Devos, S. Robijns, C. Van Goethem, I. Khalil, M. Dusselier, Interzeolite Conversion and the Role of Aluminum: Toward Generic Principles of Acid Site Genesis and Distributions in ZSM-5 and SSZ-13, Chem. Mater. 33 (2021) 2516–2531. https://doi.org/10.1021/acs.chemmater.0c04832.

[30] J. Devos, M.L. Bols, D. Plessers, C. Van Goethem, J.W. Seo, S.J. Hwang, B.F. Sels, M. Dusselier,

Journal Pre-proofs

Synthesis–Structure–Activity Relations in Fe-CHA for C–H Activation: Control of Al Distribution by Interzeolite Conversion, Chem. Mater. 32 (2020) 273–285. https://doi.org/10.1021/acs.chemmater.9b03738.

[31] M.A. Camblor, A. Corma, S. Valencia, Synthesis in fluoride media and characterisation of aluminosilicate zeolite beta, J. Mater. Chem. 8 (1998) 2137–2145. https://doi.org/10.1039/a804457k.

[32] C. Baerlocher, L.B. McCusker, Database of Zeolite Structures. Accessed on 2020 02 12, Available at: Http://Www.Iza-Structure.Org/Databases/ (Accessed On. (2014).

[33] O. Pachtová, M. Kocirik, A. Zikánová, B. Bernauer, S. Miachon, J.A. Dalmon, A comparative study of template removal from silicalite-1 crystals in pyrolytic and oxidizing regimes, Microporous Mesoporous Mater. 55 (2002) 285–296. https://doi.org/10.1016/S1387-1811(02)00430-4.

[34] K.H. Gilbert, R.M. Baldwin, J.D. Way, The Effect of Heating Rate and Gas Atmosphere on Template Decomposition in Silicalite-1, (2001) 4844–4849.

[35] S. Higuchi, I. Tsukada, Pulsed-laser deposition of LiNbO3 thin films at low oxidation gas pressure with pure ozone, Japanese J. Appl. Physics, Part 2 Lett. 42 (2003) L1066. https://doi.org/10.1143/jjap.42.l1066.

[36] E. Bourgeat-Lami, F. Di Renzo, F. Fajula, P.H. Mutin, T. Des Courieres, Mechanism of the thermal decomposition of tetraethylammonium in zeolite β, J. Phys. Chem. 96 (1992) 3807–3811. https://doi.org/10.1021/j100188a044.

[37] M. Soulard, S. Bilger, H. Kessler, J.L. Guth, DTA-GC-MS coupling for the characterization of the volatile products resulting from the decomposition of organic templates occluded in zeolites, Thermochim. Acta. 204 (1992) 167–178. https://doi.org/10.1016/0040-6031(92)80325-Q.

[38] X. Gao, C.Y. Yeh, P. Angevine, Mechanistic study of organic template removal from ZSM-5

Journal Pre-proofs

precursors, Microporous Mesoporous Mater. 70 (2004) 27–35. https://doi.org/10.1016/j.micromeso.2004.02.014.

[39] M. Soulard, S. Bilger, H. Kessler, J.L. Guth, Thermoanalytical characterization of MFI-type zeolites prepared either in the presence of OH- or of F- ions, Zeolites. 7 (1987) 463–470. https://doi.org/10.1016/0144-2449(87)90016-9.

[40] Levenspiel Octave, Chemical Reaction Engineering, 3rd ed., Wiley, 1999. https://www.wiley.com/en-us/Chemical+Reaction+Engineering%2C+3rd+Edition-p-9781119628705 (accessed July 2, 2021).

[41] G.J. Hutchings, R.G. Copperthwaite, T. Themistocleous, G.A. Foulds, A.S. Bielovitch, B.J. Loots, G. Nowitz, P. Van Eck, A comparative study of reactivation of zeolite Y using oxygen and ozone/oxygen mixtures, Appl. Catal. 34 (1987) 153–161. https://doi.org/10.1016/S0166-9834(00)82452-5.

[42] S.P. Tekade, D.Z. Shende, K.L. Wasewar, Hydrogen generation in an annular micro-reactor: An experimental investigation and reaction modelling by shrinking core model (SCM), Int. J. Chem. React. Eng. 16 (2018). https://doi.org/10.1515/ijcre-2017-0202.

[43] R.J. Morrissey, C.C.S.J. Schubert, The reactions of ozone with propane and ethane, Combust. Flame. 7 (1963) 263–268. https://doi.org/10.1016/0010-2180(63)90191-3.

[44] X. Gao, Y. Zhang, S. Adusumilli, J. Seitzman, W. Sun, T. Ombrello, C. Carter, The effect of ozone addition on laminar flame speed, Combust. Flame. 162 (2015) 3914–3924. https://doi.org/10.1016/j.combustflame.2015.07.028.

[45] R. Lee, M.L. Coote, Mechanistic insights into ozone-initiated oxidative degradation of saturated hydrocarbons and polymers, Phys. Chem. Chem. Phys. 18 (2016) 24663–24671. https://doi.org/10.1039/c6cp05064f.

[46] X. Wang, Y. Guo, L. Yang, X. Cheng, The Application and Reaction Mechanism of Catalytic

Journal Pre-proofs

Ozonation in Water Treatment, J Env. Anal Toxicol. 2 (2012) 150. https://doi.org/10.4172/2161-0525.1000150.

[47] X. Li, D. Wang, S. Zhang, Evaluation of Fe-Functionalized 4A Zeolite as Ozone Catalyst for an Enhancement of Hydroxyl Radical Pathway in a Multiphase Reactor, Ozone Sci. Eng. 41 (2019) 156–165. https://doi.org/10.1080/01919512.2018.1510764.

[48] B. Legube, N. Karpel Vel Leitner, Catalytic ozonation: A promising advanced oxidation technology for water treatment, Catal. Today. 53 (1999) 61–72. https://doi.org/10.1016/S0920-5861(99)00103-0.

[49] L. Forni, D. Bahnemann, E.J. Hart, Mechanism of the hydroxide ion initiated decomposition of ozone in aqueous solution, J. Phys. Chem. 86 (1982) 255–259. https://doi.org/10.1021/j100391a025.

[50] H. Chen, O.A. Abdelrahman, Cooperative Adsorption: Solvating the Hofmann Elimination of Alkylamines, ACS Catal. (2021) 6416–6430. https://doi.org/10.1021/acscatal.1c01364.

[51] I. Jirka, P. Sazama, A. Zikánová, P. Hrabánek, M. Kocirik, Low-temperature thermal removal of template from high silica ZSM-5. Catalytic effect of zeolitic framework, Microporous Mesoporous Mater. 137 (2011) 8–17. https://doi.org/10.1016/j.micromeso.2010.08.015.

[52] Q. Qian, D. Mores, J. Kornatowski, B.M. Weckhuysen, Template removal processes within individual micron-sized SAPO-34 crystals: Effect of gas atmosphere and crystal size, Microporous Mesoporous Mater. 146 (2011) 28–35. https://doi.org/10.1016/j.micromeso.2011.05.024.

[53] F. Muñoz, C. Von Sonntag, The reactions of ozone with tertiary amines including the complexing agents nitrilotriacetic acid (NTA) and ethylenediaminetetraacetic acid (EDTA) in aqueous solution, J. Chem. Soc. Perkin Trans. 2. (2000) 2029–2033. https://doi.org/10.1039/b004417m.

Journal Pre-proofs

[54] M. Liu, J. Li, Z. Liu, Y. Zhao, N. Jiang, Y. Wu, Improve low−temperature selective catalytic reduction of NOx with NH 3 by ozone injection, Int. J. Plasma Environ. Sci. Technol. 14 (2020) 1007–1018. https://doi.org/10.34343/ijpest.2020.14.e01007.

[55] R.T. Carr, M. Neurock, E. Iglesia, Catalytic consequences of acid strength in the conversion of methanol to dimethyl ether, J. Catal. 278 (2011) 78–93. https://doi.org/10.1016/j.jcat.2010.11.017.

Journal Pre-proofs